batteries

MDPI

Article

Learning the Ageing Behaviour of Lithium-Ion Batteries Using Electric Vehicle Fleet Analysis

Thomas Lehmann *, Erik Berendes, Richard Kratzing and Gautam Sethia

Fraunhofer Institute for Transportation and Infrastructure Systems, 01069 Dresden, Germany; gautam.sethia@ivi.fraunhofer.de (G.S.)
* Correspondence: thomas.lehmann@ivi.fraunhofer.de

Abstract: This article presents the results of the Febal project, where the aim was to parametrize a stress-factor-based ageing model for Lithium-ion batteries using operation data of an electric fleet. Contrary to state-of-the-art methods, this approach does not rely on laboratory ageing tests only. Instead, a novel physics-informed learning procedure is used to combine the accuracy and flexibility of data-driven approaches with the extrapolation properties of physical models. The ageing model is parameterized in a two-stage process. In order to cover data ranges not present in operation, a laboratory ageing test campaign is used as a baseline. In the second stage, transfer learning is used to adjust a subset of the model parameters to fit data of different cells. This approach is not only applied to laboratory measurements but also validated by a series of capacity checkup tests performed with a fleet of electric vehicles. Results show the improved state-of-health (SOH) prediction of the proposed model parameterization method.

Keywords: field data; informed neural network; battery ageing

Citation: Lehmann, T.; Berendes, E.; Kratzing, R.; Sethia, G. Learning the Ageing Behaviour of Lithium-Ion Batteries Using Electric Vehicle Fleet Analysis. *Batteries* **2024**, *10*, 432. https://doi.org/10.3390/batteries10120432

Academic Editor: Ottorino Veneri

Received: 21 October 2024
Revised: 15 November 2024
Accepted: 3 December 2024
Published: 5 December 2024

1. Introduction

The performance degradation of lithium-ion cells, especially within the context of automotive applications, poses significant challenges that are closely studied by both researchers and industry stakeholders. Accurate prediction of the ageing behaviour of lithium-ion batteries is essential for improving the performance, safety, and longevity of electric vehicles (EVs). As such, numerous research efforts have been dedicated to understanding and modelling the factors that contribute to battery degradation over time. The prediction of the ageing behaviour of lithium-ion batteries is addressed in various research activities, an overview of which is given in [1]. Most of these studies deal with laboratory data and often focus on specific ageing effects. Semi-empirical functions are commonly used to fit ageing test data. A comprehensive overview of empirical ageing models can be found in [2,3]. The generalization of these models and the application to other cell types is studied in [4]. As a result, it can be stated that the optimal model structure depends on cell type as well as on the operation profile.

Recently, the detailed investigation of ageing modes has gained a lot of attention in research [5–8], where attempts to estimate cell intrinsic/physical states are carried out. This leads to deeper understanding of ageing states and enhances ageing prediction. Neural networks have also proven to be effective in several state-of-health (SOH) prediction scenarios. In [9], a combination of a convolution neural network (CNN) and a long short-term memory (LSTM) neural network is used to predict accelerated ageing. In [10], the application of bidirectional LSTM networks for capacity prediction is analysed.

Regardless of the model approach, comprehensive datasets of aged batteries under various operation conditions are needed for accurate parameterization. In [11], an overview of the design of an experiment as well as its application to experimental battery ageing investigation is given. Based on the presented theory, several ageing test campaigns are also evaluated. Unfortunately, open public datasets are very rare (in [12] an overview of available

datasets is given). The transferability of laboratory experiments to field data is stated as one of the key challenges in battery state estimation in [13]. On the one hand, some causes of ageing that are relevant in practice, such as mechanical stress and imbalances in cells, have not been adequately investigated in the laboratory [14]. On the other hand, some conditions (e.g., extreme temperature effects) rarely occur in field data and should therefore be tested in the laboratory instead. In order to parameterize ageing models from multiple data sources or to apply models to other cell types, transfer learning methods can be used. An overview of the recent progress in battery state estimation using transfer learning is provided in [15]. In [16], transfer learning is used for calendric ageing prediction of different cell types. In [17], a cycle synchronization method is proposed in order to transfer ageing state information between cells. Most of the recent studies still focus on laboratory data only. In [18], a neural network model is trained with data derived from an operation. In [19], SOH estimation is performed using datasets from various electric vehicles. However, the combination of field and laboratory data is barely investigated in the literature.

In this article, a novel hybrid learning approach, developed within the Febal project [20], is proposed in order to make optimal use of both data sources, laboratory data and operational data. Herein, aspects from physics-informed neural networks as well as from transfer learning are combined (see Section 2.2.1). An empirical ageing model analogous to [21] is coupled to a feedforward neural network to enhance prediction accuracy (see Section 2.2). The aim is to guarantee good extrapolation properties while also preserving the flexibility and prediction accuracy of neural networks. A fleet of electric buses was monitored by us for several years and checked using regular capacity tests. The data were transferred in a specifically designed monitoring system. Furthermore, laboratory ageing tests of cells with similar cell chemistry were analysed in our lab facility (see Section 2.1). Our approach estimates stress maps, mapping operation conditions to ageing effects using laboratory data (see Section 2.3.1). Customized transfer learning approaches are thereafter applied to predict the ageing of other cell chemistries (see Section 3.2) and the electric vehicle fleet (see Section 3.3). The results show the superiority of the proposed hybrid model approach to commonly used empirical relationships and highlights the opportunities of using field data for model parameterization.

2. Materials and Methods

2.1. Datasets

The four datasets summarized in Table 1 are used in this study. There are three laboratory ageing campaigns and a dataset recorded from a fleet of electrical buses. The laboratory ageing data primarily consist of constant current experiments under fixed conditions. This means temperature, SOC range, and current rates are kept fixed. In the field data, these values are inherently dynamic. Another difference is the number of conducted checkup tests. Whereas in laboratory tests all cells are regularly examined in dedicated checkup tests, this cannot be realized in real electric vehicle fleets due to high investment of time and effort. Here, only some vehicles have undergone a dedicated charge and discharge procedure from which "ground truth" capacity values can be determined.

Exemplary checkup results of the calendric experiments of the Sony campaign are shown in Figure 1. The decline in capacity follows the same qualitative square-root-like pattern but with different ageing rates. In the other laboratory campaigns, linear ageing trends are also observed.

Figure 2 shows the range of important battery parameters for each bus of the entire bus fleet. It can be seen that the usage profiles are quite similar. Thermal management keeps the cells at comfortable temperatures during most of the operation phase, with some outliers at the start or during fast charging. The range of the SOC is also very similar. Buses are operated above 60% SOC most of the time. Charge rate and monthly full cycles differ based on the used charging station and driven route.

Table 1. Summary of the used datasets.

Name	Source	Operation Conditions of the Cell	Number of Cells/Vehicles
Sony	TUM [22]	• 5 °C–60 °C • SOC: 5–100%	97
batteries 2020	EU project [23]	• 25 °C–45 °C • SOC: 20–100%	146
Kokam	IVI (internal, unpublished)	• 10 °C–40 °C • SOC: 25–100%	28
vehicle fleet	transportation company	• 25 °C–30 °C • SOC: 40–100%	38

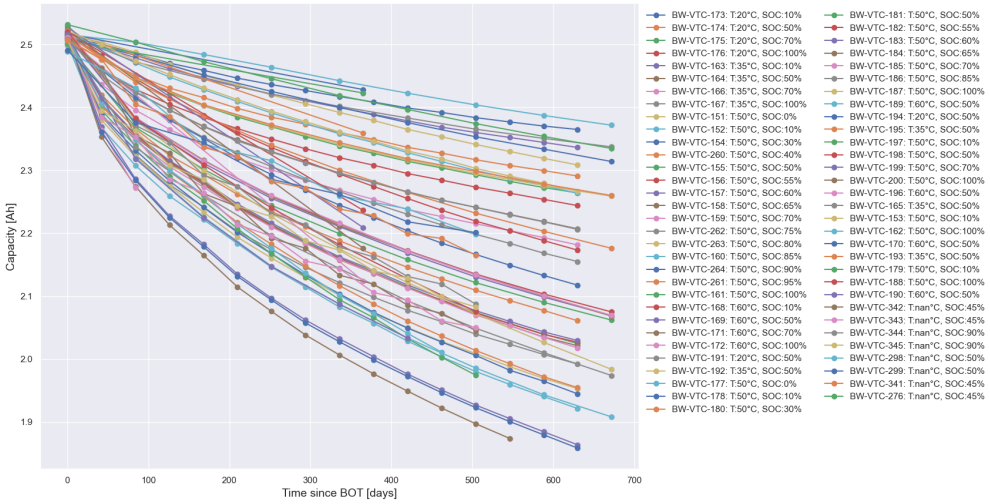

Figure 1. Determined capacities during calendric experiments of the Sony ageing test campaign as a function of time since beginning of testing (BOT).

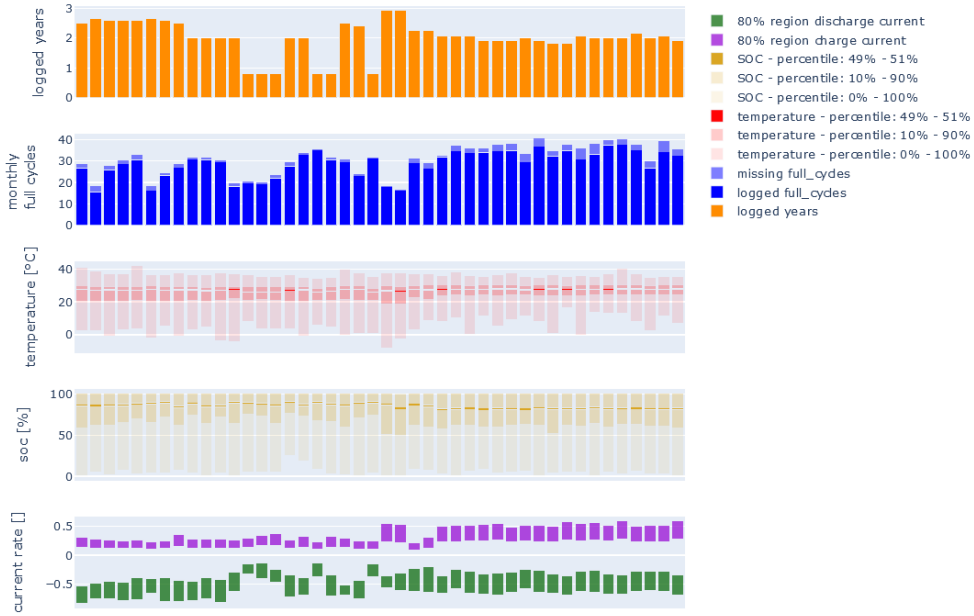

Figure 2. Usage profile of the buses of the fleet. Each entry represents one bus. The second top plot shows the mean monthly full cycles. The plot below indicates the distribution of temperature and SOC. The bottom plot shows the current range during operation as well as during charging.

2.2. Ageing Model Structure

The aim of the ageing model is the prediction of capacity fade (and resistance increase) under various operation conditions. State-of-the-art approaches include simple Ah counting up to physical modelling of ageing phenomena. An overview of degradation mechanisms and prediction algorithms is presented in [24].

Since the ageing behaviour depends strongly on the cell used and the operating conditions, the models must be parameterized on the basis of ageing tests. So far, only laboratory data have been used for this task. To accomplish this, a suitable model structure is necessary. An approach based on stress maps as proposed in [3] is used here. These types of models are also refereed to as weighted Ah models [25]. The resulting model structure is sketched in Figure 3.

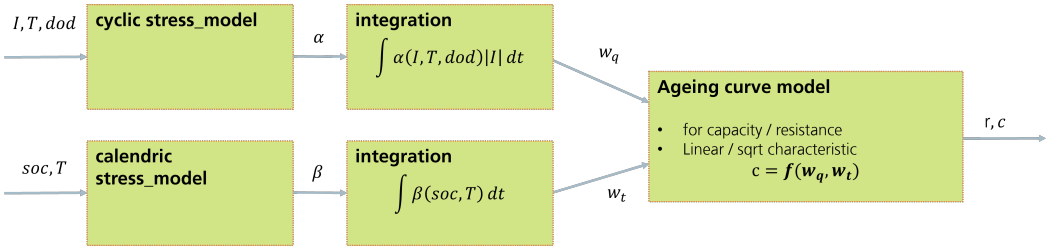

Figure 3. Structure of prediction model.

The ageing model consists of three submodels. The inputs and outputs are listed in Table 2. The parameters that can be trained depend on the approach used and are explained in more detail in the corresponding Sections 2.2.1 and 2.2.2.

Table 2. Inputs and outputs of the submodels.

Submodel	Inputs	Output	Trainable Parameter
calendric stress model	$x = [soc, T]$	$y = \beta$	weights Θ_β or parameter $p_9, \ldots, p_{13}$
cyclic stress model	$x = [T, dod, I]$	$y = \alpha$	weights Θ_α or parameter $p_0, \ldots, p_8$
ageing curve model	$x = [w_q, w_t]$	$y = c$	l_q and l_t

The main equations are as follows:

$$w_q(t) = \frac{1}{2C_{nom}} \int_{t_0}^{t} \alpha(I(t'), T(t'), dod(t'))|I(t')|dt' \quad (1)$$

$$w_t(t) = \frac{1}{S_y} \int_{t_0}^{t} \beta(soc(t'), T(t'))dt' \quad (2)$$

$$c(t) = f_{ac}(w_q(t), w_t(t)) = c_0 - (c_0 - c_{eol}) \cdot \left(\sqrt{\frac{w_q(t)}{l_q}} + \sqrt{\frac{w_t(t)}{l_t}} \right) \quad (3)$$

The value α describes the stress level of the operation during usage. It is used as a weighting factor for the charge throughput. The input dependencies are restricted to depth of discharge (DOD), temperature, and current. SOC is not used as an input due to complications in the parametrization process (see Section 2.3.1) and empirical observations. Analogue β indicates the calendric stress level. Integration of α and β over time using Equations (1)–(3) results in the weighted equivalent full cycles w_q and the weighted lifetime w_t, respectively. The factor $2C_{nom}$ is used for scaling to full cycles and the factor S_y is used for scaling to years.

The ageing curve f_{ac} is used to calculate the predicted capacity from these values. Here, a square-root ageing behaviour is assumed, as the checkup results (see Figure 1) indicate.

c_{eol} is the capacity at end of life, which is typically set to 80% of the initial capacity c_0. l_q is the cycle life in equivalent full cycles and l_t the calendric lifetime in years. The ageing curve depends heavily on the cell chemistry and must therefore be adapted. As explained in Section 2.3.3, transfer learning is used for this purpose.

The crucial point is the calculation of the cyclical and calendar stress factors. Various approaches are used in this thesis, including both a function-based model and a neural network. Details of these models are described in the following Sections 2.2.1 and 2.2.2. These two models are coupled using the approach described in Section 2.3.2. The resulting ageing model is referred to as a "coupled neural network" in this article.

In Section 3.3, a simple equal stress model is also used for benchmark purposes. Stress factors α and β are set to one regardless of operation conditions in this model. As the focus is on capacity estimation, the ageing models are limited to the prediction of capacity. However, they can be extended to predict resistance values.

2.2.1. Function-Based Stress Model

This model uses known functional relationships between the stress factors α and β and operation features (SOC, temperature, dod, and current rate). For temperature, the Arrhenius law is used. Depth of discharge as well as state of charge are modelled using a linear function. Piecewise linear interpolation is used for the current. The vector $I = (I_0, \ldots, I_4)$ is used to specify the grid points. I_0 is the maximal discharge current and I_4 the maximal charge current. Using these values, differences between charge (positive current) and discharge (negative current) as well as the absolute value of the current are taken into account.

$$\begin{aligned}
\alpha_T(T) &= p_0 + p_1 e^{p_2 T} && (4)\\
\alpha_{dod}(dod) &= p_2 + p_3 \cdot dod && (5)\\
\alpha_I(I) &= \begin{cases} p_4 + \frac{p_5 - p_4}{I_1 - I_0} \cdot (I - I_0) & I_0 < I \leq I_1 \\ \cdots & \\ p_7 + \frac{p_8 - p_7}{I_4 - I_3} \cdot (I - I_3) & I_3 < I \leq 4 \end{cases} && (6)\\
\beta_T(T) &= p_9 + p_{10} e^{p_{11} T} && (7)\\
\beta_{soc}(soc) &= p_{12} + p_{13} \cdot soc && (8)
\end{aligned}$$

The model contains a total of 14 parameters, which are combined to form the vector $p = (p_0, \ldots, p_{13})$. The resulting cyclic and calendric stress are obtained by multiplying the single stress factors (as proposed in [26]):

$$\begin{aligned}
\alpha(T, dod, I) &= \alpha_T(T) \cdot \alpha_{dod}(dod) \cdot \alpha_I(I) \\
\beta(T, soc) &= \beta_T(T) \cdot \beta_{soc}(soc) && (9)
\end{aligned}$$

2.2.2. Neural Network Stress Model

Two feedforward neural networks (FFNNs) are used to obtain calendric and cyclic stress factors from input features $x = [T, dod, I]$. The network structure is sketched in Figure 4.

A similar neural network is used to predict the calendric stress value β. This means functions (9) are replaced by

$$\begin{aligned}
\alpha(T, dod, I) &= f_\alpha(T, dod, I; \Theta_\alpha) \\
\beta(T, soc) &= f_\beta(soc, T; \Theta_\beta) && (10)
\end{aligned}$$

Here, Θ_α and Θ_β represent the weights of the two FFNNs. Since there are only a few input features and no exotic inter-dependencies, the network should be able to capture the information obtained from the given ageing test data. In order to guarantee positive stress values, activity regularization is used. Due to its superior mathematical

properties, including differentiability, boundness, stationarity, and smoothness, the GELU activation function was used (see [27]). Information about thee number of nodes and further hyperparameters is given in Table 3.

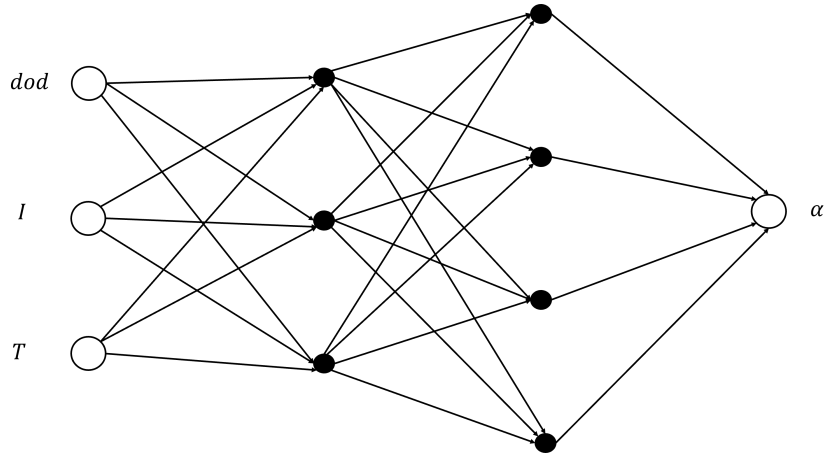

Figure 4. Structure of FFNN for cyclic stress value α. The number of nodes in each layer, the activation function, and further hyperparameters are listed in Table 3.

Table 3. Hyperparameters of the neural networks.

Parameter	Description	Value
n_{cal}	number of nodes in each layer of the calendric stress neural network	[5, 5]
n_{cyc}	number of nodes in each layer of cyclic stress neural network	[8, 8]
a	activation function	GELU
λ_{nonneg}	regularization constant for positive output values	1.0

2.3. Parametrization of Ageing Models

2.3.1. Using Laboratory Measurements

Since operation conditions are kept constant within the experiments, Equation (1) simplifies to

$$c(T, \overline{soc}, dod, I_c, I_d, a_q, a_t) = c_0 - (c_0 - c_{eol}) \left(\sqrt{\frac{a_q}{l_q}} \cdot \sqrt{\frac{\alpha(I_c, T, dod) + \alpha(I_d, T, dod)}{2}} + \sqrt{\frac{a_t}{l_t}} \sqrt{\beta(\overline{soc}, T)} \right) \tag{11}$$

$$a_t = \frac{t}{S_y} \tag{12}$$

$$a_q = \frac{t}{2C_{nom}} \int |I| dt = \frac{t}{2C_{nom}} \cdot \frac{I_c + |I_d|}{2} \tag{13}$$

Here, a_q denotes the (unweighted) equivalent full cycles and a_t the lifetime of the battery. It must also be emphasized that operation conditions are kept fixed; this is obviously not possible for SOC and current during cyclic experiments. This must be considered within the integration. Degradation effects during charging and discharging are superimposed. Hence, the charging current I_c as well as the discharge current I_d appear in the final Equation (11). SOC changes linearly with time in cyclic experiments. Nevertheless, analytical integration can be challenging if complex SOC dependencies are considered. In addition to empirical observations, this is one reason why the SOC is only taken into account for calendric ageing. Furthermore, a linear function is used (see Equation (8)). The solution of the integral therefore leads to the use of the mean SOC ($\overline{soc}$) in the calculation of the calendric stress factor.

These calculations and considerations lead to a fairly simple equation for predicting the capacity from ageing test experiments. All integrations are solved analytically, which is a great benefit for subsequent parameter optimization. Nevertheless, the equation is valid for cyclic and calendar tests, allowing both stress models to be parameterized together. There is no need for a two-stage fitting approach (first calendar ageing and then cyclic ageing), which is commonly performed.

From Equation (11), it can be seen that there is a degree of freedom in determining the calendar and cycle life parameters l_q and l_t (multiplying l_t as well as β with same factor will not change the predicted capacity). This is used to specify reference conditions for which $\beta(soc_r, T_r) = 1$ and $\alpha(I_r, T_r, dod_r) = 1$ hold. The used reference conditions are listed in Table 4.

Table 4. Reference conditions.

Parameter	Value
soc_r	0.8
T_r	25 °C
dod	0.3
I_r	−0.5

2.3.2. Coupling of Function-Based Model and Neural Network

Neural networks or even lookup tables have great potential in accurately predicting stress map functions α and β. However, a large number of experiments/cells would be needed to ensure good extrapolation behaviour.

With physics-informed neural networks, a similar problem is tackled [28]. Neural networks are combined with physical equations to gain good extrapolation properties but still preserve good fit capability to data. Therefore, the presented functional stress model is coupled with the feedforward neural networks presented in Section 2.2.2. Instead of only considering the deviation of J_{data} from training data, a second term is added to the loss function J. This term describes the deviation between the two models at specified collocation points. These collocation points span a dense grid of conditions where neural networks will predict valid results. In summary, the following four vectors are involved in the calculation of the cost function:

- $c_{t,m}$: capacities obtained during checkup tests;
- $c_{t,nn}$: capacities predicted by neural networks under experiment conditions;
- $c_{col,em}$: capacities predicted by an empirical model for collocation points;
- $c_{col,nn}$: capacities predicted by neural networks for collocation points.

And the used loss function reads as follows:

$$J(c_{t,m}, c_{t,nn}, c_{col,em}, c_{col,nn}) = J_{data}(c_{t,m}, c_{t,em}) + \lambda_{pinn} \cdot J_{col}(c_{col,em}, c_{col,nn}) \quad (14)$$

The second term J_{col} describes the deviation of the neural network from the functional model output at collocation points $c_{col,em}$. Through minimizing this loss function, a good fit to training data as well as good extrapolation behaviour is obtained. J_{col} basically serves as a regularization term that couples the functional model with the neural network and prevents overfitting.

As usual, the mean squared error is used for both loss functions. For J_{data}, the sum of overall training points is taken; for J_{col}, collocation points are used.

The Tensorflow framework is used to create and train the ageing model, including the collocation loss term. The established Adam algorithm (see [29]) is used for optimization.

2.3.3. Transfer Learning

Transfer learning (TL) is used if a model exists for a general task, but needs to be adapted to a specific application. Here, it is assumed that the stress level is the same for

different cells. However, both the cycle and calender lifetimes as well as the ageing characteristics (linear or quadratic ageing) differ considerably between different cell chemistries. To take this into account, the ageing curve of the model is fitted to the cell under consideration. If laboratory ageing tests are available, the same procedure as described in Section 2.3.1 (but with fixed stress map weights) can be used.

The situation is somewhat different when field data are used for this purpose. Here, the operating conditions such as temperature and current are not kept constant, but change rapidly. Hence, the integral in Equation (1) does not vanish and must be calculated using numerical approaches. To speed this up, histogram-based methods (see [30]) are used. As a result, weighted full cycles $w_{q,i}$ and weighted lifetime values $w_{t,i}$ are obtained at each checkup position. They can be used as input values to fit the ageing curve parameters l_q and l_t by minimizing

$$\sum_{i}^{N} \left(f_{ac}(w_{q,i}, w_{t,i}; l_q, l_t) - c_i \right)^2 \rightarrow \min \tag{15}$$

Here, c_i are the estimated capacities from the checkup tests.

3. Results

3.1. Estimated Stressmaps

In this section, the resulting stress maps for the presented model structures are discussed. The Figures 5–7 show the fit results for the calendric model part. It can be seen that the function model is suitable for extrapolation, whereas the neural network gives unreasonable values at conditions not covered by ageing tests.

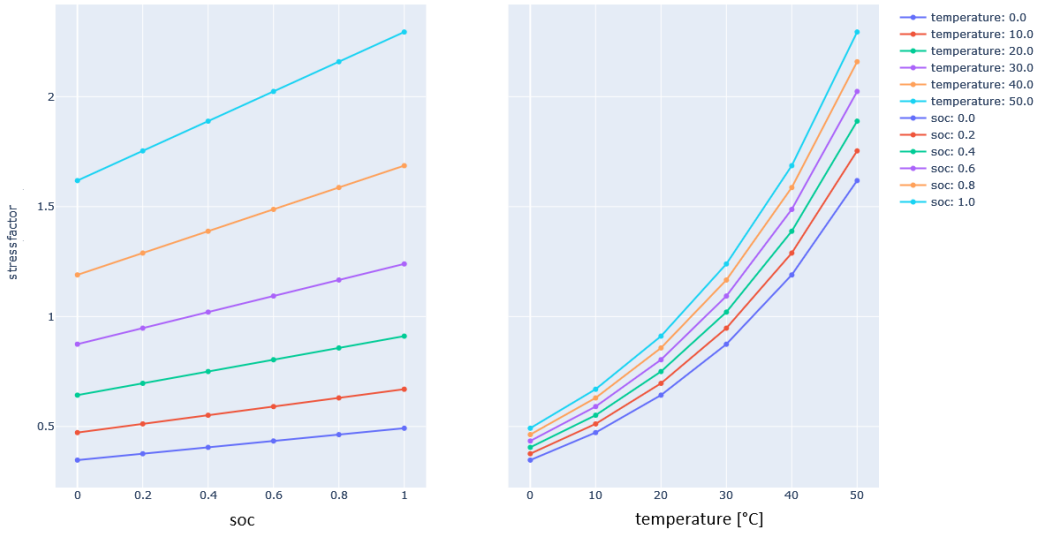

Figure 5. Calendric stress map obtained from function-based model. The values are sensible and allow good extrapolation over the whole temperature and SOC range.

Figure 8 compares the prediction results of the three models. As expected, the neural network produces the lowest prediction error. On the other hand, extrapolation performance for unobserved data is poor. One indicator for this is the smoothness of the stress map, defined as the inverse of the integral of the hessian (see [31]):

$$S(\beta) = \frac{1}{\int \frac{\partial \beta(soc,T)}{\partial soc \partial T} dsocdT} \tag{16}$$

Low values of this metric indicate a rugged stress map and potential overfitting. Thus, extrapolation performance will also be poor in general. A summary of RMSE as well as smoothness is given in Table 5. The coupled neural network is a compromise between the function-based model and the neural network: it offers good extrapolation properties and

good prediction accuracy. For the cyclic part, the deviation between the function model and coupled neural network is larger (see Appendix A). That indicates that the coupled approach significantly increases the prediction accuracy compared to the functional model.

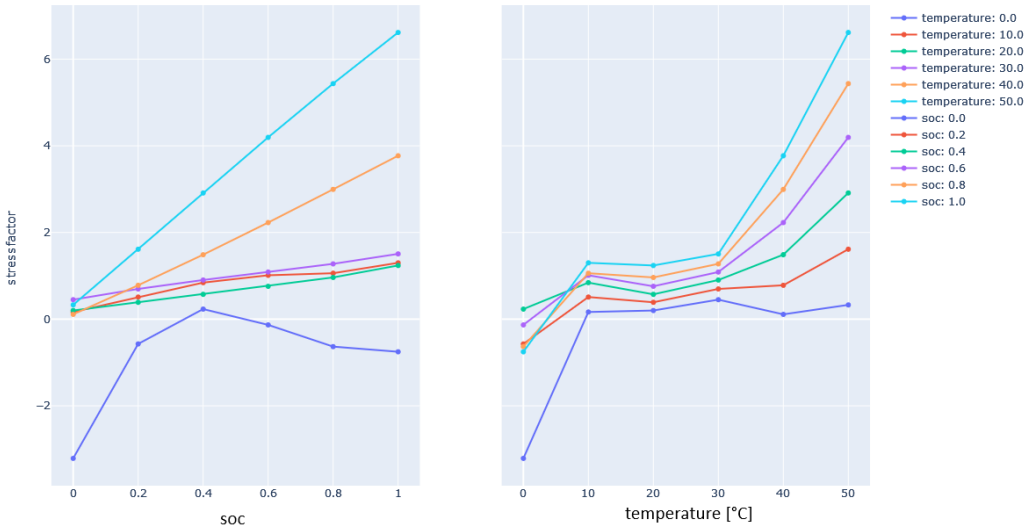

Figure 6. Calendric stress map obtained from neural network. Main trends and relationships are as expected. However, for some operating conditions (e.g., at a temperature of 0 °C) for which no experiments were carried out, the values are not meaningful. Therefore, the stress map is not suitable for extrapolation to conditions that are not included in the training dataset.

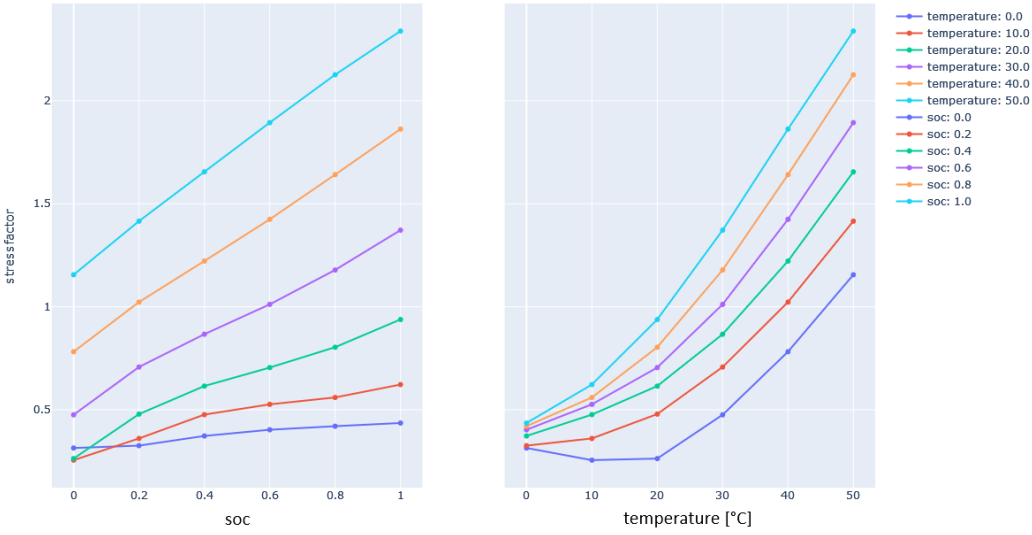

Figure 7. Calendric stressmap obtained from coupled model. There are only slight deviations from the function-based model. This means that this model is already capable of modelling calendric ageing with good accuracy.

Table 5. Capacity prediction error for training data and smoothness metric for stress maps.

Model	RMSE	Max Error	Stressmap Smoothness
function-based model	5.4%	19.1%	9.5
neural network	2.3%	11.1%	0.3
coupled neural network	4.5%	16.9%	0.9

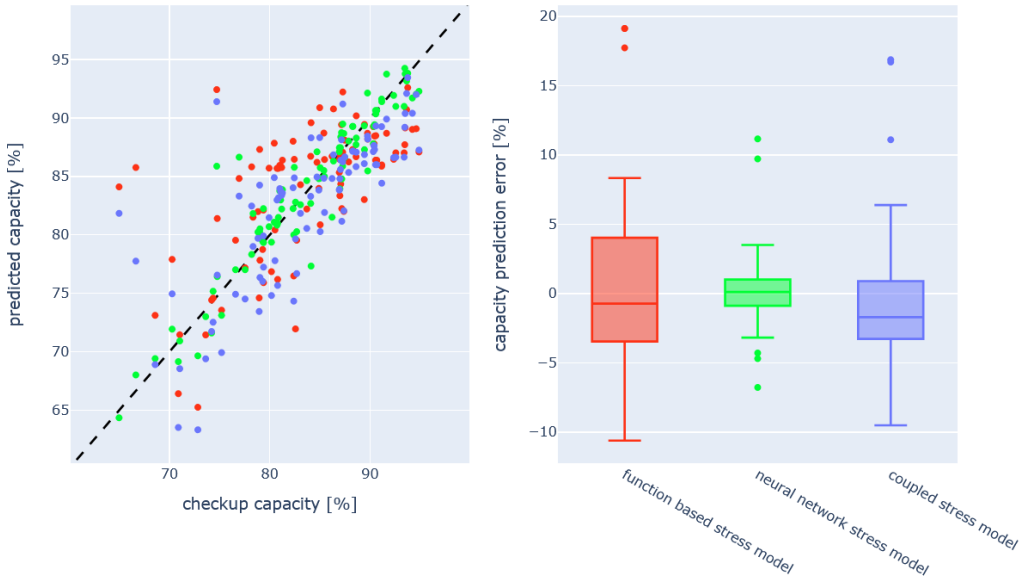

Figure 8. (**left**) Prediction results of the three models for the used training dataset plotted against the target checkup test capacities. (**right**) Box plot of prediction error.

3.2. Application to Other Cell Chemistries

In order to validate the generalization properties of the estimated stress map, it was applied to the laboratory ageing test campaigns listed in Table 1. Here, dedicated capacity checkup tests were performed at regular intervals.

In the first step, the ageing model was parameterized using the Sony dataset and applied to the batteries 2020 and the Kokam ageing test campaigns (see Section 2.1). As described in Section 2.3.3, the cycle life and calendar life parameters of the ageing curve model were adjusted before predicting the capacity. The result is shown in Figure 9. The standard deviation of the prediction error (summarized in Table 6) is around 5% for both ageing test campaigns and within the same magnitude as for the training dataset. This confirms the analysis performed in [32], which states that general ageing effects can be transferred between cell chemistries.

Table 6. Capacity prediction error for investigated measurement campaigns.

Campaign	RMSE	Max Error
Sony (training dataset)	4.5%	16.9%
Kokam	5.3%	14.3%
batteries 2020	5.0%	10.8%

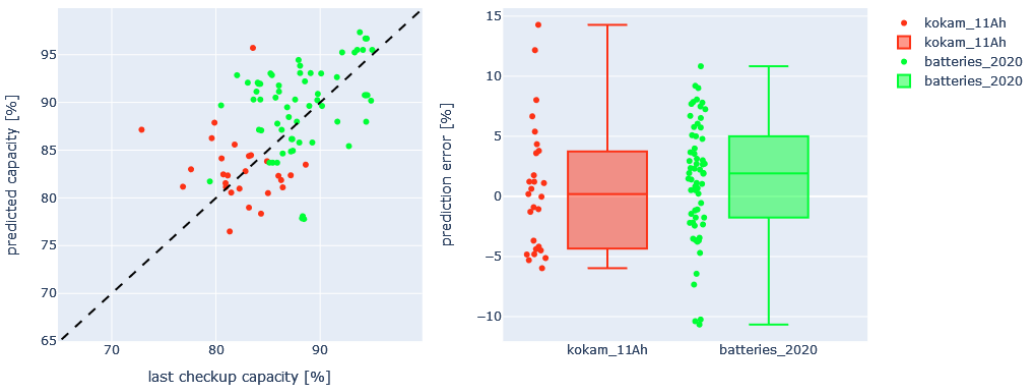

Figure 9. Plot of determined capacity at checkups compared to the prediction of the coupled neural network. Prediction error is slightly higher than on training dataset (see Figure 8).

3.3. Application to Electric Vehicle Fleet

The capacities for the field data checkups were predicted as outlined in Section 2.3.3. As a benchmark, two further prediction methods were applied. In summary, the following algorithms are compared:

- Equal stress model: instead of using stress maps to evaluate the operation conditions, only the pure lifetime a_t and equivalent full cycles a_q are used.
- Coupled neural network without transfer learning: the coupled neural network without adjustment to field data checkup tests is used. This means that the transfer learning step is skipped.
- Coupled neural network with transfer learning: the coupled neural network with adjustment to field data checkup tests is used.

The results are shown in Figure 10 and summarized in Table 7. It can be seen that the coupled neural network is superior to the equal stress model. The use of transfer learning to adapt to the different cell chemistries improves the estimation. Whereas the other models overestimate the capacity fade, the prediction errors are distributed around zero for this approach.

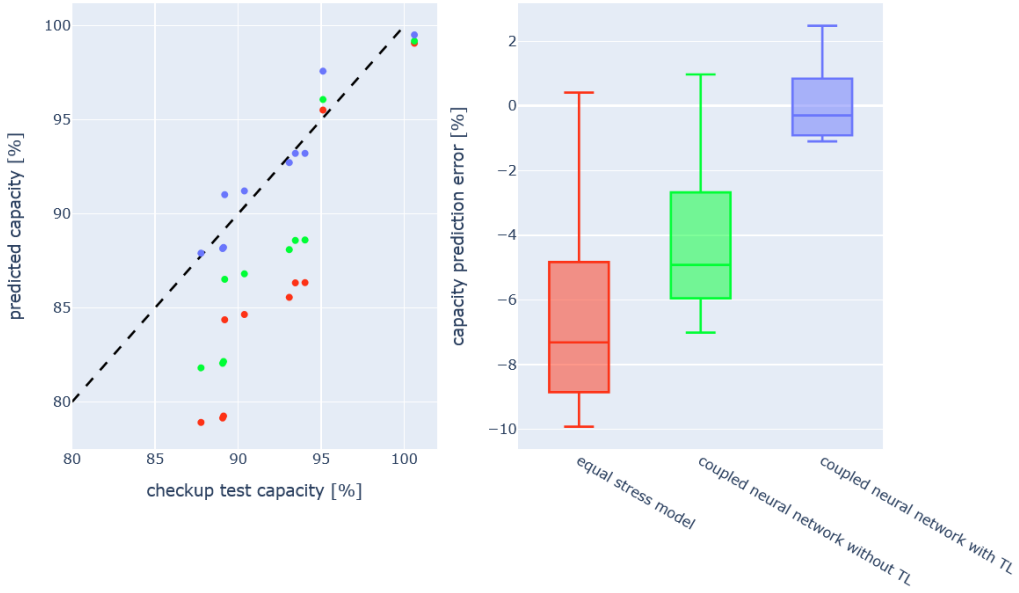

Figure 10. Plot of measured capacity at checkups compared to the predicted capacity using three different approaches. Field-data-tuned stress map provides lowest prediction error.

Table 7. Capacity prediction error for electric vehicle fleet.

Campaign	RMSE	Max Error
equal stress model	7.1%	9.9%
coupled neural network without TL	4.8%	7.0%
coupled neural network with TL	1.2%	2.5%

4. Discussion

Previous publications have investigated the transferability of ageing models between cell chemistries on the basis of laboratory data. This study extends this approach, as it shows how laboratory ageing test data may be combined with field data in order to improve capacity prediction and thereby the end-of-life prognosis of Li-ion batteries. Validation was enabled by conducting reference tests on multiple vehicles of an electric fleet.

The usage of neural networks coupled to function-based models was applied to create accurate but also reliable stress maps. In particular, extrapolation outside the–often sparse–ageing test data is ensured. Transfer learning techniques were used to adapt cell-specific

ageing characteristics. The transfer of general, extensively studied ageing effects from laboratory measurements to field data have proven to be feasible.

Future work should extend the usage of field data. For instance, SOH estimations could be used instead of time- and cost-intensive checkup tests.

Author Contributions: Conceptualization, T.L.; methodology, T.L. and E.B.; software, T.L.; validation, T.L. and E.B.; formal analysis, T.L.; investigation, T.L.; resources, E.B. and R.K.; data curation, R.K.; writing—original draft preparation, T.L.; writing—review and editing, T.L., E.B. and G.S.; visualization, T.L.; supervision, T.L. and R.K.; project administration, R.K.; funding acquisition, R.K. All authors have read and agreed to the published version of the manuscript.

Funding: We gratefully acknowledge the financial support by Bundesministerium für Bildung und Forschung (BMBF 03XP0308A).

Data Availability Statement: The data presented in this study are available on request from the corresponding author on reasonable request. The data are not publicly available due to privacy policies.

Conflicts of Interest: The authors declare no conflicts of interest.

Abbreviations

The following abbreviations are used in this manuscript:

SOC	State of Charge
DOD	Depth of Discharge
SOH	State of Health
FFNN	Feedforward Neural Network
TL	Transfer Learning
RMSE	Root Mean Squared Error
IVI	Institute for Transportation and Infrastructure Systems

Appendix A

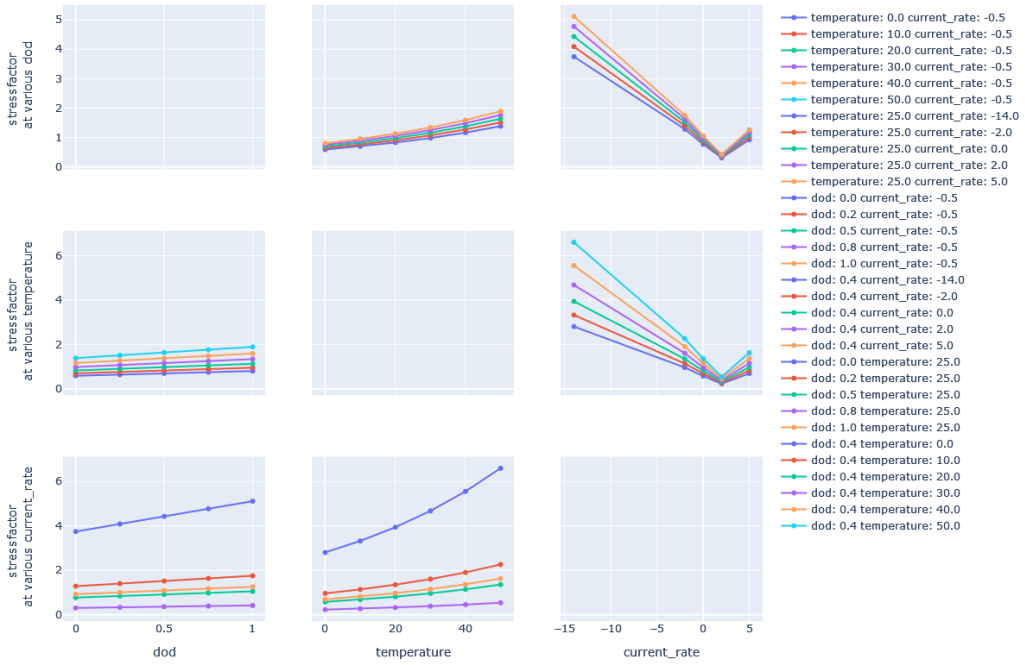

Figure A1. Cyclic stress map obtained from function-based model.

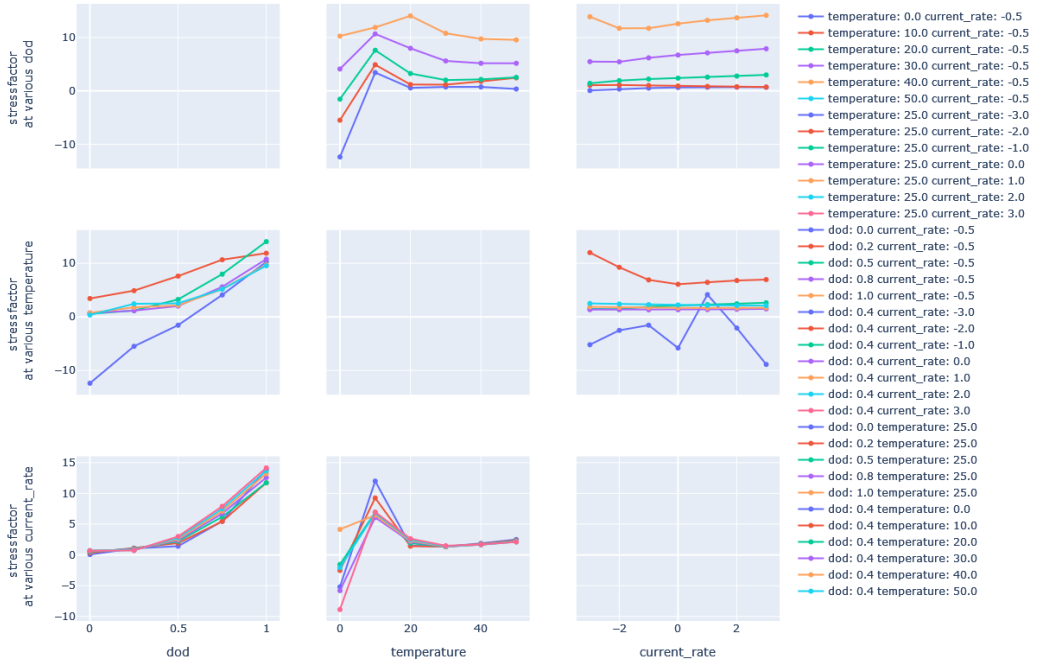

Figure A2. Cyclic stress map obtained from neural network.

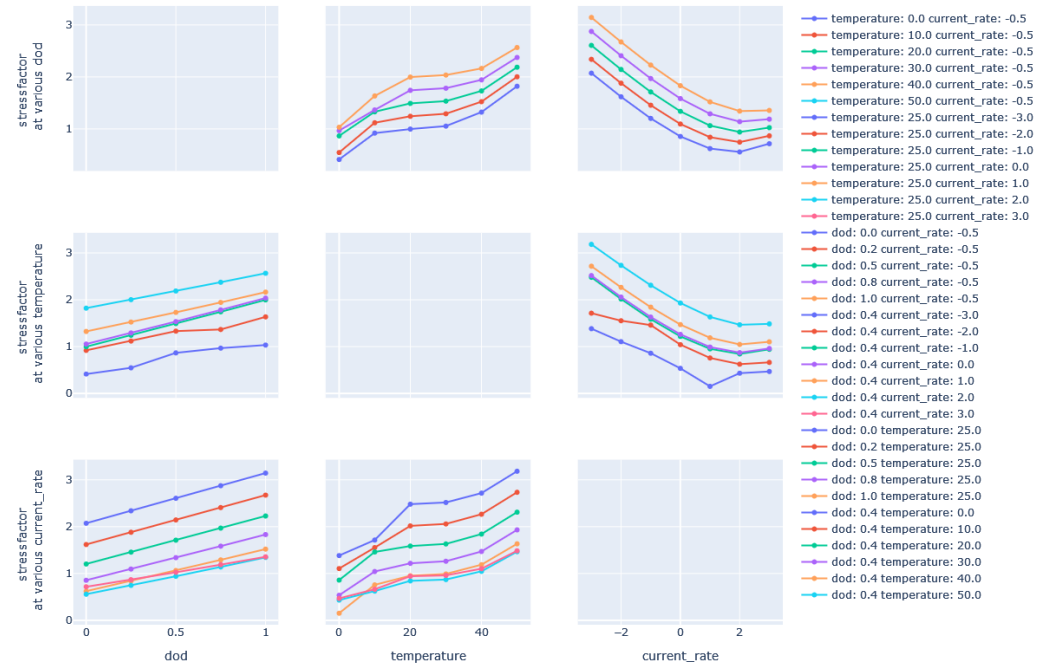

Figure A3. Cyclic stress map obtained from coupled model.

References

1. Liao, Z.; Lv, D.; Hu, Q.; Zhang, X. Review on Aging Risk Assessment and Life Prediction Technology of Lithium Energy Storage Batteries. *Energies* **2024**, *17*, 3668. [CrossRef]
2. Gewald, T.; Candussio, A.; Wildfeuer, L.; Lehmkuhl, D.; Hahn, A.; Lienkamp, M. Accelerated Aging Characterization of Lithium-ion Cells: Using Sensitivity Analysis to Identify the Stress Factors Relevant to Cyclic Aging. *Batteries* **2020**, *6*, 6. [CrossRef]
3. Vermeer, W.; Member, S.; Mouli, G.R.C.; Bauer, P. A Comprehensive Review on the Characteristics and Modeling of Lithium-Ion Battery Aging. *IEEE Trans. Transp. Electrif.* **2022**, *8*, 2205–2232. [CrossRef]
4. Heimhuber, P. Parametrisierung und Evaluierung von Alterungsmodellen für NMC- und NCA- basierte Lithium-Ionen-Batterien. Diploma Thesis, TU Dresden, Dresden, Germany, 2022.

5. Birkl, C.; Roberts, M.R.; McTurk, E.; Bruce, P.G.; Howey, D.A. Degradation diagnostics for lithium ion cells. *J. Power Sources* **2017**, *341*, 373–386. [CrossRef]
6. Schmitt, J.; Schindler, M.; Oberbauer, A.; Jossen, A. Determination of degradation modes of lithium-ion batteries considering aging-induced changes in the half-cell open-circuit potential curve of silicon–graphite. *J. Power Sources* **2022**, *532*, 231296. [CrossRef]
7. Xu, R.; Wang, Y.; Chen, Z. Data-Driven Battery Aging Mechanism Analysis and Degradation Pathway Prediction. *Batteries* **2023**, *9*, 129. [CrossRef]
8. Smith, A.J.; Svens, P.; Varini, M.; Lindbergh, G.; Lindström, R.W. Expanded In Situ Aging Indicators for Lithium-Ion Batteries with a Blended NMC-LMO Electrode Cycled at Sub-Ambient Temperature. *J. Electrochem. Soc.* **2021**, *168*, 110530. [CrossRef]
9. Che, Y.; Zheng, Y.; Forest, F.E.; Sui, X.; Hu, X.; Teodorescu, R. Predictive health assessment for lithium-ion batteries with probabilistic degradation prediction and accelerating aging detection. *Reliab. Eng. Syst. Saf.* **2024**, *241*, 109603. [CrossRef]
10. Xu, X.; Tang, S.; Han, X.; Lu, L.; Wu, Y.; Yu, C.; Sun, X.; Xie, J.; Feng, X.; Ouyang, M. Fast capacity prediction of lithium-ion batteries using aging mechanism-informed bidirectional long short-term memory network. *Reliab. Eng. Syst. Saf.* **2023**, *234*, 109185. [CrossRef]
11. Román-Ramírez, L.; Marco, J. Design of experiments applied to lithium-ion batteries: A literature review. *Appl. Energy* **2022**, *320*, 119305. [CrossRef]
12. Mayemba, Q.; Mingant, R.; Li, A.; Ducret, G.; Venet, P. Aging datasets of commercial lithium-ion batteries: A review. *J. Energy Storage* **2024**, *83*, 110560. [CrossRef]
13. Sulzer, V.; Mohtat, P.; Aitio, A.; Lee, S.; Yeh, Y.T.; Steinbacher, F.; Khan, M.U.; Lee, J.W.; Siegel, J.B.; Stefanopoulou, A.G.; et al. The challenge and opportunity of battery lifetime prediction from field data. *Joule* **2021**, *5*, 1934–1955. [CrossRef]
14. von Bulow, F.; Meisen, T. A review on methods for state of health forecasting of lithium-ion batteries applicable in real-world operational conditions. *J. Energy Storage* **2023**, *57*, 105978. [CrossRef]
15. Liu, K.; Peng, Q.; Che, Y.; Zheng, Y.; Li, K.; Teodorescu, R.;Widanage, D.; Barai, A. Transfer learning for battery smarter state estimation and ageing prognostics: Recent progress, challenges, and prospects. *Adv. Appl. Energy* **2023**, *9*, 100117. [CrossRef]
16. Azkue, M.; Lucu, M.; Martinez-Laserna, E.; Aizpuru, I. Calendar Ageing Model for Li-Ion Batteries Using Transfer Learning Methods. *World Electr. Veh. J.* **2021**, *12*, 145. [CrossRef]
17. Zhou, K.Q.; Qin, Y.; Yuen, C. Transfer-Learning-Based State-of-Health Estimation for Lithium-Ion BatteryWith Cycle Synchronization. *IEEE/ASME Trans. Mechatron.* **2022**, *28*, 692–702. [CrossRef]
18. von Bulow, F.; Mentz, J.; Meisen, T. State of health forecasting of Lithium-ion batteries applicable in real-world operational conditions. *J. Energy Storage* **2021**, *44*, 103439. [CrossRef]
19. Li, S.; He, H.; Zhao, P.; Cheng, S. Health-Conscious vehicle battery state estimation based on deep transfer learning. *Appl. Energy* **2022**, *316*, 119120. [CrossRef]
20. BMBF. Battnutzung-Cluster. 2022. Available online: https://www.battnutzung-cluster.de/de/projekte/febal/ (accessed on 29 March 2023).
21. Krupp, A. Semi-Empirical Aging Model for Predicting the Capacity Loss of Lithium-Ion Batteries in Stationary Storage Systems. Doctoral Dissertation, Carl von Ossietzky Universität Oldenburg, Oldenburg, Germany, 2023.
22. Wildfeuer, L.; Karger, A.; Aygül, D.;Wassiliadis, N.; Jossen, A.; Lienkamp, M. Experimental degradation study of a commercial lithium-ion battery. *J. Power Sources* **2023**, *560*, 232498. [CrossRef]
23. Timmermans, J.M.; Nikolian, A.; De Hoog, J.; Gopalakrishnan, R.; Goutam, S.; Omar, N.; Coosemans, T.; Van Mierlo, J.; Warnecke, A.; Sauer, D.U.; et al. Batteries 2020—Lithium-ion battery first and second life ageing, validated battery models, lifetime modelling and ageing assessment of thermal parameters. In Proceedings of the 2016 18th European Conference on Power Electronics and Applications (EPE'16 ECCE Europe), Karlsruhe, Germany, 5–9 September 2016; pp. 1–23. [CrossRef]
24. Hu, X.; Xu, L.; Lin, X.; Pecht, M. Battery Lifetime Prognostics. *Joule* **2020**, *4*, 310–346. [CrossRef]
25. Redondo-Iglesias, E.; Venet, P.; Pelissier, S. Modelling Lithium-Ion Battery Ageing in Electric Vehicle Applications—Calendar and Cycling Ageing Combination Effects. *Batteries* **2020**, *6*, 14. [CrossRef]
26. Xu, B.; Oudalov, A.; Ulbig, A.; Andersson, G.; Kirschen, D.S. Modeling of Lithium-Ion Battery Degradation for Cell Life Assessment. *IEEE Trans. Smart Grid* **2018**, *9*, 1131–1140. [CrossRef]
27. Lee, M. Mathematical Analysis and Performance Evaluation of the GELU Activation Function in Deep Learning. *J. Math.* **2023**, *1*, 4229924. [CrossRef]
28. Cuomo, S.; Cola, V.D.; Giampaolo, F.; Rozza, G.; Raissi, M.; Piccialli, F. Scientific Machine Learning Through Physics–Informed Neural Networks: Where we are and What's Next. *J. Sci. Comput.* **2022**, *92*, 88. [CrossRef]
29. Kingma, D.P.; Ba, J.L. Adam: A method for stochastic optimization. *arXiv* **2017**, arXiv:1412.6980.
30. Zdravevski, E.; Lameski, P.; Mingov, R.; Kulakov, A.; Gjorgjevikj, D. Robust histogram-based feature engineering of time series data. In Proceedings of the 2015 Federated Conference on Computer Science and Information Systems (FedCSIS), Lodz, Poland, 13–16 September 2015; pp. 381–388. [CrossRef]

31. Chen, X.; Tong, Z.; Liu, H.; Cai, D. Metric learning with two-dimensional smoothness for visual analysis. In Proceedings of the 2012 IEEE Conference on Computer Vision and Pattern Recognition 2012, Providence, RI, USA, 16–21 June 2012; pp. 2533–2538. [CrossRef]
32. Deletang, T.; Barnel, N.; Franger, S.; Assaud, L. Transposition of a weighted ah-throughput model to another li-ion technology: Is the model still valid? New insights on the mechanisms. In Proceedings of the International Conference on Computational Methods for Coupled Problems in Science and Engineering, Rhodes Island, Greece, 12–14 June 2017.